Journal of Materials Chemistry A

Synthesis of Ternary PtPdCu Spheres with Three-Dimensional Nanoporous Architectures toward Superior Electrocatalysts

Journal:	*Journal of Materials Chemistry A*
Manuscript ID:	TA-COM-04-2015-002951.R3
Article Type:	Paper
Date Submitted by the Author:	20-Jul-2015
Complete List of Authors:	JIANG, Bo; National Institute for Materials Science, WPI Center for MANA Cuiling, Li; National Institute for Materials Science, WPI Center for MANA Malgras, Victor; National Institute for Materials Science, WPI Center for MANA Yamauchi, Yusuke; National Institute for Materials Science, WPI Center for MANA

Journal of Materials Chemistry A

ARTICLE

Synthesis of Ternary PtPdCu Spheres with Three-Dimensional Nanoporous Architectures toward Superior Electrocatalysts

Received 00th January 20xx,
Accepted 00th January 20xx

DOI: 10.1039/x0xx00000x

www.rsc.org/

Bo Jiang,[a,b] Cuiling Li,*[a] Victor Malgras,[a] and Yusuke Yamauchi*[a,b]

We report a simple method for the preparation of ternary PtPdCu spheres with three-dimensional (3D) nanoporous structure in solution phase. The structure, composition, and electronic states of the obtained material are characterized and studied by various physical techniques. By varying the amount of Cu precursor involved in the reaction, the composition of spheres can be adjusted without affecting the morphology. Due to the nanoporous structure and the multimetallic synergetic effect, our ternary nanoporous PtPdCu spheres exhibited 1.7, 2.8, and 4.9 times higher activity than that of binary nanoporous PtPd sphere, dendritic Pt, and commercial Pt black catalysts, respectively.

1. Introduction

Platinum (Pt) catalysts have attracted considerable attention because they are effective catalysts for both anodic oxidation (e.g., methanol, hydrogen) and cathodic reduction (oxygen) in fuel cells.[1] However, the commercialization of fuel cells has been seriously obstructed by the slow kinetics of cathodic reactions, the poor stability, and the high cost of non-replaceable Pt.[2] Considerable efforts have been made in developing Pt-based catalysts with high performance while using a minimal amount of Pt.[3] One of the promising strategies is to introduce nonprecious metals into Pt catalyst to form multicomponent Pt-based composites, such as random/intermetallic alloys or core-shell structures, owing to the modification of the electronic structure and the rearrangement of surface atoms with different components.[4] Recently, many studies have revealed that Pt-based ternary catalysts with tuneable compositions have enhanced electrocatalytic activity toward fuel cells compared to their unitary or binary counterparts. For instance, Qu *et al.* reported a two-step synthesis of ternary Pt/PdCu nanoboxes by the hydrothermal method at relative high temperature. The catalytic activity of ternary Pt/PdCu nanoboxes toward ethanol oxidation was 6 times enhanced in comparison with that of the PdCu catalysts. The probable reason is the synergetic effect between the individual components in the ternary system.[4a] Recently, ultrathin one-dimensional ternary PtPdTe nanowires synthesized by using Te wires as template exhibited an enhanced Pt mass activity toward methanol oxidation reaction, which is 2.4 times higher than that of binary PtTe catalyst.[5] Similar results have been observed with other ternary catalysts such as FePtAu, PtNiFe, PtAuRu, and so on.[6] Thus, developing novel Pt-based ternary catalysts is currently one of the most effective strategies to enhance the usage efficiencies.

On the other hand, it has been well-established that the performances of catalysts can be affected depending of their morphology, sizes, compositions, and porous structures. Among these nanostructures, three-dimensional (3D) nanoporous structures are proved to be effective constructions to achieve a high catalytic performance.[7] This 3D nanoporous structure consists of interconnected metallic nanoparticles embedded in the pore walls, offering large surface areas, abundant active sites, and facilitate diffusion of reactant/product species. In addition, self-standing nanoporous structures are less vulnerable to aggregation and dissolution than nanoparticles during the catalytic progress. For instance, dendritic platinum nanostructures favor high catalytic performance and utilization efficiency owing to their high surface areas and lower densities.[1c] Liu *et al.* reported a strategy for the synthesis of PtRh alloy with a 3D nanoporous structure which have a better catalytic activity and durability than Pt black.[4b] Despite great advances in 3D nanoporous structure, however, only a few facile methods for creating ternary metal catalysts with 3D nanoporous structures have been reported so far because of the difficulties encountered in kinetic control of nucleation/growth in the multiple metal precursors and the limitation in formation of concave metallic porous structures.[8] Therefore, the development of a facile and effective route for large-scale preparation of Pt-based

[a] World Premier International (WPI) Research Center for Materials Nanoarchitectonics (MANA), National Institute for Materials Science (NIMS), 1-1 Namiki, Tsukuba, Ibaraki 305-0044 (Japan)
[b] Faculty of Science and Engineering, Waseda University, 3-4-1 Okubo, Shinjuku, Tokyo 169-8555 (Japan)
E-mails: Li.Cuiling@nims.go.jp; Yamauchi.Yusuke@nims.go.jp

Electronic Supplementary Information (ESI) available: [details of any supplementary information available should be included here]. See DOI: 10.1039/x0xx00000x

ternary catalyst with 3D porous nanostructure is still an urgent matter to be addressed.

In the present work, we report a facile strategy for synthesizing ternary PtPdCu spheres with a 3D nanoporous structure by aqueous one-pot method. Unlike high temperature-based and organic solvent-based approaches, our strategy is consistent with the requirements of green chemistry as only water is used as solvent. More importantly, we combine the respective advantages of ternary hetero-structure and 3D nanoporous structure to achieve maximal catalytic performance. Compared with binary nanoporous PtPd catalyst, dendritic Pt catalyst and Pt black catalyst, the ternary nanoporous PtPdCu catalyst exhibited 1.7, 2.8 and 4.9 times higher electrochemical activity, respectively.

2. Experimental

2.1. Preparation of ternary nanoporous PtPdCu spheres

In a typical synthesis of ternary nanoporous PtPdCu spheres, 1.5 ml Na_2PdCl_4 (20.0 mM), 1.5 ml H_2PtCl_6 (20.0 mM), 1.5 ml $CuCl_2$ (20 mM), 0.2 ml HCl solution (6.0 M) and 50.0 mg Pluronic F127 were mixed. After dissolving F127 under sonication, an aqueous solution of 2.0 ml ascorbic acid (0.1 M) was added to the aforementioned solution, giving a 0.03 mmol of Na_2PdCl_4, H_2PtCl_6 and $CuCl_2$ in an equimolar ratio. Then, the mixed solution was kept in an oil bath for 4 h at 95 ^oC. The residual Pluronic F127 was removed by several consecutive washing/centrifugation cycles with ethanol and water. Finally, the sample was collected by centrifuging at 14000 rpm for 20 min. The as-prepared sample was stored in ethanol until the time of use and then dried at room temperature.

2.2. Preparation of bimetallic nanoporous PtPd spheres

The synthesis of nanoporous PtPd spheres was similar to the synthesis of nanoporous PtPdCu spheres except without addition of $CuCl_2$. 1.5 ml Na_2PdCl_4 (20.0 mM), 1.5 ml H_2PtCl_6 (20.0 mM), 0.1 ml HCl solution (6.0 M) and 50.0 mg Pluronic F127 were mixed. After dissolving F127 under sonication, an aqueous solution of 2.0 ml ascorbic acid (0.1 M) was added to the aforementioned solution. Then, the mixed solution was kept in an oil bath for 4 h at 95 ^oC. The residual Pluronic F127 was removed by several consecutive washing/centrifugation cycles with ethanol and water. Finally, the sample was collected by centrifuging at 14000 rpm for 20 min. The as-prepared sample was stored in ethanol until the time of use and then dried at room temperature.

2.3. Preparation of dendritic Pt nanoparticles

The dendritic Pt nanoparticles were prepared by a wet chemical reduction process reported previously.[9] Firstly, an aqueous solution consisting of nonionic Brij58 surfactant was prepared under stirring. Then, K_2PtCl_4 and ascorbic acid (AA) were added to the surfactant Brij58 solutions, making the final concentration of K_2PtCl_4 and AA to be 5 mM and 12.5 mM, respectively. The final concentration of Brij58 in solution was 0.5 %. Then, the reaction solution was incubated without any external treatment for 12 h at room temperature. Finally, the sample was collected by centrifugation at 14000 rpm for 20 min and the residual Brij58 was removed by several consecutive washing/centrifugation cycles with ethanol and water. The as-prepared sample was stored in ethanol and then dried at room temperature.

2.4. Catalyst characterization

Scanning electron microscopy (SEM) characterizations were carried out using a Hitachi SU-8000 microscope operated at 5 kV. Transmission electron microscopy (TEM) and high-angle annular dark-field scanning TEM (HAADF-STEM) characterizations were carried out using a JEOL JEM-2100F operated at 200 kV equipped with an energy-dispersive spectrometry analyzer. The samples for TEM and HRTEM characterizations were prepared by depositing a drop of the diluted colloidal suspension on a grid. Wide-angle powder X-ray diffraction (XRD) spectrum was acquired with a Rigaku Rint 2500 diffractometer with monochromated Cu KR radiation. Low-angle XRD profiles were obtained by using a NANO VIEWER (Rigaku, Japan) equipped with a Micro Max-007 HF high-intensity micro-focus rotating anode X-ray generator. X-ray photoelectronic spectroscopy (XPS) spectra were carried out at room temperature by using a JPS-9010TR (JEOL) instrument with an Mg Kα X-ray source. All the binding energies were calibrated via referencing to C 1s binding energy (284.6 eV).

2.5. Electrochemical Characterization

Cyclic voltammograms (CV) and chronoamperometric (CA) experiments were performed using a CHI 842B electrochemical analyzer (CHI Instruments, USA). A conventional three-electrode cell was used, including an Ag/AgCl (saturated KCl) reference electrode, a platinum wire as a counter electrode, and a modified glassy carbon electrode (GCE) as a working electrode. The modified GCE was coated with as-produced samples (5.0 μg) and dried at room temperature. Then, 5.0 μl of Nafion (0.05 wt %) was coated on the surface of the modified GCE and dried before electrochemical experiments. Prior to electrochemical measurements, the GCE modified with the as-prepared sample was activated electrochemically by cycling the electrode potential between -0.2 V and +1.5 V (vs Ag/AgCl) in 0.5 M H_2SO_4 until the obtained CVs became characteristic of a clean Pt electrode. Methanol electro-oxidation measurements were performed in a solution of 0.5 M H_2SO_4 containing 0.5 M methanol at a scan rate of 50 mV s^{-1}. Mass current densities were normalized by the loaded Pt amount, which were determined by inductively coupled plasma mass spectroscopy (ICP-MS).

3. Results and discussion

The nanoporous structure of the obtained samples was firstly studied by scanning electron microscope (SEM). Well dispersed nanoporous spheres with uniform size and a diameter of 115 ± 15 nm can be observed over the entire area (Figure 1a). The highly magnified SEM image (Figure 1b) shows

that well-defined nanopores are uniformly distributed over the particle surface. The structure of the samples is further investigated by TEM. Figure 1c-d reveals that the pore walls are composed of a multitude of interconnected small nanoparticles with an average size of 5 nm. Even at the particle center, sponge-like nanoporous structures are formed. It also be seen from diffraction spots with arcs in the selected-area electron diffraction (SAED) that the sample is highly polycrystalline (Figure 1c inset).

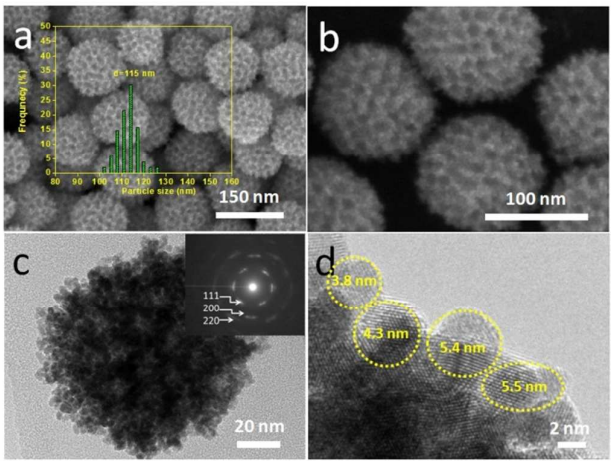

Figure 1. a) Low magnification SEM image and particle size distribution, b) high magnification SEM image, c) TEM image, d) HRTEM image of typical nanoporous PtPdCu spheres. The inset in pannel (c) is the SAED pattern obtained from the single PtPdCu sphere.

SEM and TEM observations are powerful tools for determining the nanoporous structures, even though these data remain "local". In order to get the average information from the entire sample, the PtPdCu spheres are characterized by low-angle XRD patterns. A broad peak in the low-angle region (d = 17.5 nm) was observed, corresponding to the periodicity (i.e., pore-to-pore distance) of the nanoporous structure in the obtained sample (Figure 2a). The nitrogen isotherm of the ternary nanoporous PtPdPt spheres gave a large surface area of 63.5 $m^2 g^{-1}$. This value is comparable or higher than those of most reported dendritic Pt catalysts and other Pt-based catalysts.[8b-d]

The wide-angle X-ray diffraction (XRD) patterns (Figure 2b) of the typical sample is characteristic of a metallic face-centered cubic (ffc) structure. No other diffraction peaks of monocomponent Cu, Pt, or Pd were observed, indicating the probable formation of single-phase alloys. Compared with standard diffraction patterns of Pd and Pt, all the diffraction peaks of PtPdCu are slightly shifted to higher angles, suggesting the substitution of the smaller Cu metal atoms.[10] The average grain size can be calculated from the (200) diffraction peak based on the Scherrer equation,[11] returning a diameter of approximately 6.0 nm, supporting the averaged nanoparticle size observed in Figure 1c. The Pt:Pd:Cu atomic ratio in the sphere measured by inductively coupled plasma mass spectrometry (ICP-MS) is ca. 38:37:25. The quasi-equimolarity of Pt and Pd suggests Pt and Pd precursors were completely reduced. On the other hand, the Cu species have not completely reacted, which may be ascribed to the Cu^{2+} species having a lower reduction potential (Cu^{2+}/Cu: +0.34 V vs. Standard Hydrogen Electrode, SHE) than that of Pt and Pd species ($[PdCl_4]^{2-}$/Pd: +0.62 V vs. SHE, $[PtCl_6]^{2-}$/$[PtCl_4]^{2-}$: +0.73 V vs. SHE, and $[PtCl_4]^{2-}$/Pt: +0.76 V vs. SHE).[4d, 12] The Cu content in the samples can be increased, however, by increasing the amount of Cu precursor in the synthesis. As a result, the XRD peaks shift linearly towards higher angles with increasing the amount of amount of Cu precursor (Figure S1). According to Vegard's law, the diffraction peak of the metal alloy with the molar composition should locate between the peaks of pure metals[13] (Figure S1a) and a linear relation exists between the crystal lattice parameter of an alloy and the content of the constituent elements (Figure S1b).[14] Therefore, we can confirm that the prepared ternary PtPdCu spheres display an alloy phase. In addition, the ternary PtPdCu spheres with a uniform porous structure could be well retained even after modifying the Cu content from 5.4% to 23.8% (Figure S2).

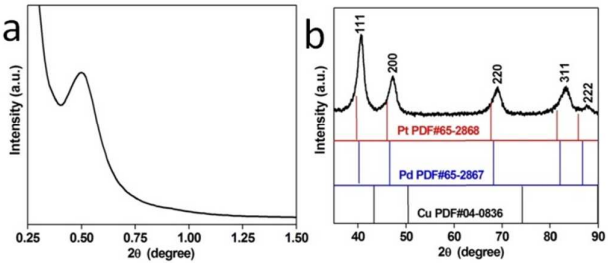

Figure 2. a) Low-angle and b) wide-angle XRD patterns of the typical nanoporous PtPdCu spheres.

The electronic states of Pd, Pt, and Cu in nanoporous PtPdCu spheres were investigated by X-ray photoelectron spectroscopy (XPS). As shown in Figure 3a, the Pt^0 4f doublet located at 71.1 eV and 74.5 eV can be observed. Figure 3b shows that the binding energy of Cu $2p_{3/2}$ and Cu $2p_{1/2}$ located at 932.1 eV and 951.8 eV can be ascribed to metallic Cu^0. It has been generally known that Cu is easily oxidized in air, but the Cu atoms in the alloy state are stable. The binding energies at 335.2 eV and 340.5 eV are assigned to the Pd $3d_{5/2}$ and Pd $3d_{3/2}$ (Figure 3c). The Pt 4f binding energy in ternary nanoporous PtPdCu spheres negatively shift (around 0.2 eV) compared to that in commercial Pt black, indicating that Pt atoms would accept a partial charge transferred (Figure 3d).[15] This change in the electronic state of Pt further confirms the formation of an alloy phase. The peaks of these elements indicate that metallic state of Pt, Pd and Cu exist in the sample.

Considering the standard reduction potentials of each precursor, it is expected that a Pt/Pd rich core is preferentially formed, followed by the growth of a Cu-rich shell in the ternary PtPdCu spheres. In the present system, however, Pd, Pt, and Cu are uniformly distributed, as shown in elemental mapping images (Figure 4). It was observed that the reduction of the Cu precursor only occurs when a second or third metal

precursor was mixed with the Cu precursor (e.g., Pd/Cu, Pt/Cu, or Pd/Pt/Cu) (Figure S3 and Figure S4). These results indicate that the reduction of Cu precursor only takes place with the trigger of the preformed noble metal nanocrystal seeds. At the initial stage, the noble metal nuclei are reduced and serve as seeds to induce the formation of Cu atoms on the surface of noble metal nuclei.[16] Afterwards, the Cu atoms mixed with the noble metal atoms through interdiffusion processes.[16b,17]

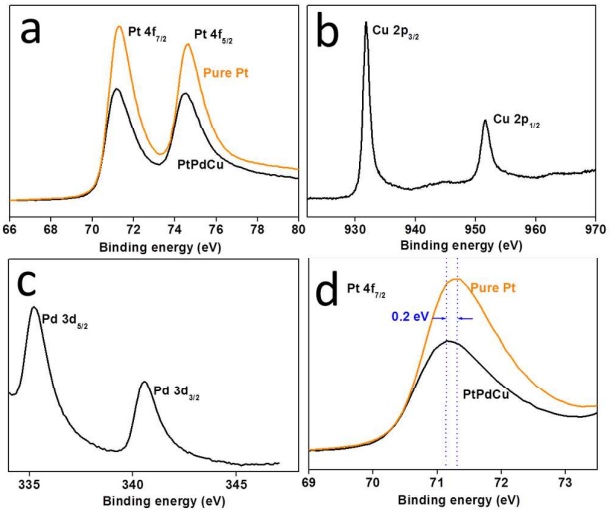

Figure 3. High resolution XPS spectra of the typical nanoporous PtPdCu spheres ((a) Pt 4f, (b) Cu 2p, (c) Pd 3d, and (d) Comparison of the XPS spectra of the Pt $4f_{7/2}$ for both PtPdCu spheres and pure Pt).

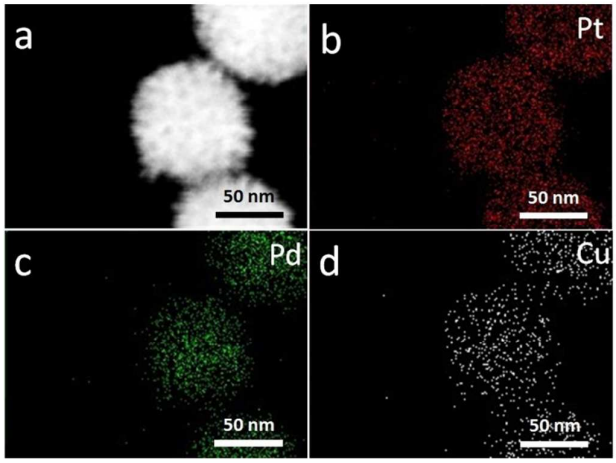

Figure 4. a) High-angle annular dark-filed scanning TEM (HAADF-STEM) showing the nanoporous structure, and b-d) elemental mapping images of the typical nanoporous PtPdCu spheres.

We further studied the time-dependent morphological change by SEM and TEM. In Figure 5a, the TEM image shows that at the beginning of the reaction (3 min), small-sized particles (around 44 nm). At this time, the nanoporous structure is not well developed on the particle surface. With increasing the reaction time, the diameter of the particles expands up to ~55 nm (Figure 5b) (30 min) then to ~78 nm (Figure 5c) (60 min). During the particle growth, the nanoporous structure becomes prominent as the particle size increases. When the reaction time is further extended to 90 min, the size of nanoparticles reaches around 115 nm (Figure 5d).

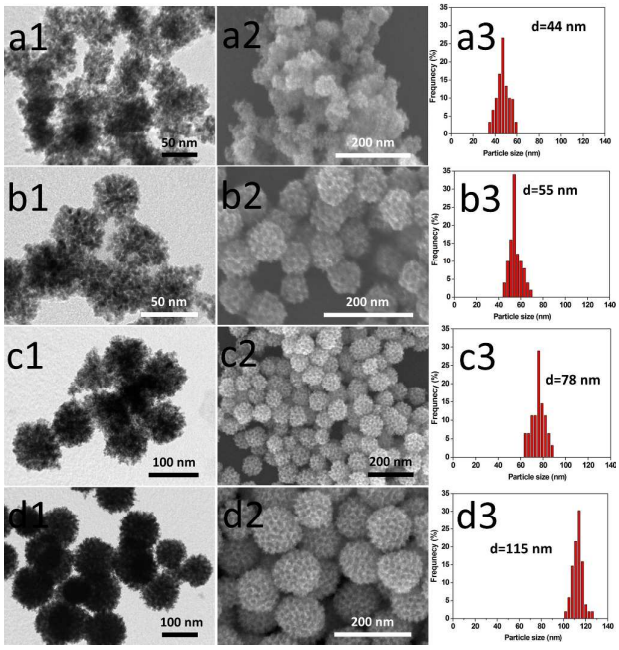

Figure 5. TEM, SEM images and particle sizes distributions of samples taken at different reaction times: a) 3 min, b) 30 min, c) 60 min and d) 90 min.

It has been recognized that F127 can be served as both stabilizing agent and pore-shaping agent during the synthesis of nanoporous oxide, nanoporous carbon, and nanoporous metals.[18] Without the addition of F127, only non-porous aggregates were obtained (Figure S5a). When a smaller amount of F127 (3 mg) was used, similar nanoporous structure was observed, but some particles were significantly aggregated (Figure S5b). Thus, the insufficient amount of F127 cannot inhibit particle aggregation effectively. When the amount of F127 was increased up to 50 mg, the desired ternary PtPdCu spheres were found without any by-products (Figure 1a). In the solution, the dissolved metal species are coordinated by water molecules to form metal-aqua complexes. The coordinated water molecules usually interact with ethylene oxide (EO) groups of the F127 micelles, as demonstrated in our previous study.[1a,8a] Therefore, the metal-aqua complexes dissolving in the solution are incorporated in the PEO shell region of the micelles. The F127 micelles can directly act as a structural directing agent. The above results reveal that the F127 play an important role in formation of both the spherical shape and the nanoporous structure.

To evaluate the performance of ternary nanoporous PtPdCu spheres, the electrochemical catalytic activity towards methanol oxidation reaction was investigated. Nanoporous PtPd spheres (Figure S6a), dendritic Pt nanoparticles (Figure S6b), and Pt black (Figure S6c) were used for comparison.

Figure 6a shows the typical cyclic voltammograms (CVs) of methanol oxidation in 0.5 M H_2SO_4 containing 0.5 M methanol solution at a scan rate of 50 mV s^{-1} on ternary nanoporous PtPdCu catalyst, binary nanoporous PtPd catalyst, dendritic Pt catalyst and Pt black catalyst. All the current densities were normalized by Pt mass (mass activity). All the catalysts exhibited typical features of methanol oxidation performance on the Pt surface. The as-prepared nanoporous ternary PtPdCu catalyst exhibit superior electrochemical activity as its current densities is 0.43 A mg^{-1}_Pt, which is about 1.7, 2.8 and 4.9 times than that of binary nanoporous PtPd (0.252 A mg^{-1}_Pt), dendritic Pt nanoparticles (0.153 A mg^{-1}_Pt), and Pt (0.087 A mg^{-1}_Pt) black catalysts, respectively. This result highly supports the assumption that ternary compositions in all-metal catalysts have higher catalytic activity than unitary or binary counterparts due to the synergetic function of individual components. Furthermore, our as-prepared ternary nanoporous PtPdCu spheres exhibited a negatively-shifted onset potential for electrochemical oxidation of methanol compared to that of binary nanoporous PtPd, dendritic Pt and Pt black catalysts, indicating that the methanol oxidation reactions were facilitated (Figure 6b). Even when the activity was normalized by electrochemical surface area (ECSA), our ternary nanoporous PtPdCu spheres (1.38 mA cm^{-2}) still exhibited the highest activity compared with binary nanoporous PtPd (1.08 mA cm^{-2}), dendritic Pt (0.84 mA cm^{-2}) and PtB (0.66 mA cm^{-2}).

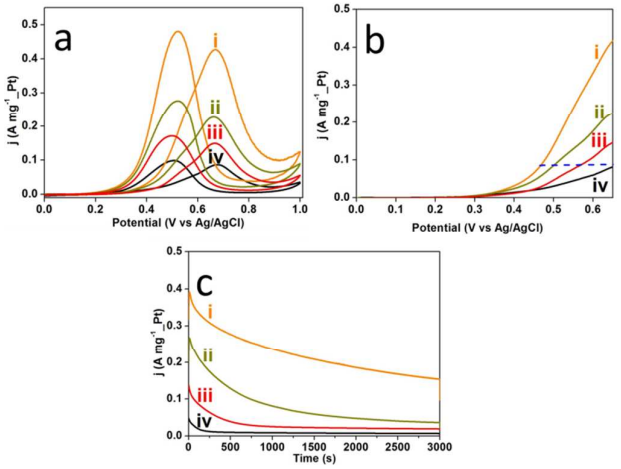

Figure 6. a) cyclic voltammograms, b) linear-sweep voltammograms, and c) chronoamperometric curves (recorded at 0.6 V) for methanol oxidation reactions catalyzed by i) nanoporous PtPdCu catalyst, ii) binary nanoporous PtPd catalyst, iii) dendritic Pt catalyst and iv) Pt black catalyst.

The origin of the enhancement in MOR for ternary nanoporous PtPdCu spheres with three-dimensional nanoporous architectures can be explained by composition and porous structure effects. Firstly, in the PtPdCu alloy system, the electronic structure modification of Pt surface by alloying with heteroatoms (*e.g.,* Cu or Pd), as demonstrated in the XPS analysis, can promote the catalytic activity,[10,19] which has been commonly observed in Pt-based alloys.[20] Second, the enhanced activity may be attributed to the nanoporous structure with very high surface area (63.5 m^2 g^{-1}) to facilitate diffusion of reactant/product species.[21]

Compared to previously reported Pt-based catalysts (Table S1), our prepared ternary nanoporous PtPdCu catalyst exhibits higher current densities, showing the potential of this material for practical electrocatalytic applications in methanol oxidation reaction. Figure 6c clearly reveals that both the ternary nanoporous PtPdCu catalyst and binary PtPd have a higher durability toward methanol oxidation compared with nanoparticles because the nanoporous structure provides a superior stability by preventing aggregation.

Conclusions

In summary, we have demonstrated a facile aqueous-phase method for the fabrication of ternary PtPdCu spheres with 3D nanoporous structure. F127 plays a critical role in formation of the porous structure and in giving a spherical morphology. The electrocatalytic activity of this catalyst toward methanol oxidation was also evaluated in comparsion with binary nanoporous PtPd and Pt black catalysts. Due to the porous effect, the ternary nanoporous PtPdCu catalyst has a superior activity than the corresponding binary nanoporous PtPd, dendritic Pt nanoparticles and Pt black catalysts. In addition, this facile and simple synthetic procedure can be extended to the fabrication of many other ternary metal catalysts by selecting appropriate precursor solutions leading to favorable compositions.

Notes and references

1 a) C. Li, T. Sato, Y. Yamauchi, *Angew. Chem. Int. Ed*. 2013, **52**, 8050-8053; b) Q. Li, P. Xu, B. Zhang, G. Wu, H. Zhao, E. Fu, H. L. Wang, *Nanoscale* 2013, **5**, 7397-7402; c) L. Wang, Y. Yamauchi, *Chem. Mater*. 2009, **21**, 3562-3569; d) X. Huang, Z. Zhao, J. Fan, Y. Tan, N. Zheng, *J. Am. Chem. Soc*. 2011, **133**, 4718-4721; e) T. Yu, D. Y. Kim, H. Zhang, Y. Xia, *Angew. Chem. Int. Ed*. 2011, **50**, 2773-2777.

2 a) B. Lim, M. Jiang, P. H. Camargo, E. C. Cho, J. Tao, X. Lu, Y. Zhu, Y. Xia, *Science* 2009, **324**, 1302-1305; b) C. Chen, Y. Kang, Z. Huo, Z. Zhu, W. Huang, H. L. Xin, J. D. Snyder, D. Li, J. A. Herron, M. Mavrikakis, M. Chi, K. L. More, Y. Li, N. M. Markovic, G. A. Somorjai, P. Yang, V. R. Stamenkovic, *Science* 2014, **343**, 1339-1343.

3 a) Y. C. Tseng, H. S. Chen, C. W. Liu, T. H. Yeh, K. W. Wang, *J. Mater. Chem. A* 2014, **2**, 4270-4275; b) H. A. Esfahani, J. Liu, M. Hu, N. Miyamoto, S. Tominaka, K. C. W. Wu, Y. Yamauchi, *Small* 2013, **9**, 1047-1051; c) C. Li, M. Imura, Y. Yamauchi, *Chem. Eur. J*. 2014, 20, 3277-3282; d) C. Hu, X. Zhai, Y. Zhao, K. Bian, J. Zhang, L. Qu, H. Zhang, H. Luo, Nanoscale 2014, **6**, 2768-2775; e) X. Niu, M. Lan, H. Zhao, C. Chen, *Chem. Eur. J*. 2013, **19**, 9534-9541.

4 a) C. Hu, H. Cheng, Y. Zhao, Y. Hu, Y. Liu, L. Dai, L. Qu, *Adv. Mater*. 2012, **24**, 5493-5498; b) Y. Zhang, M. Janyasupab, C. W. Liu, X. Li, J. Xu, C. C. Liu, Adv. *Funct. Mater*. 2012, **22**, 3570-3575; c) F. Taufany, C. J. Pan, J. Rick, H. L. Chou, M. C. Tsai, B. J. Hwang, D. G. Liu, J. F. Lee, M. T. Tang, Y. C. Lee, C. I. Chen, *ACS Nano* 2011, **5**, 9370-9381.

5 H. H. Li, S. Zhao, M. Gong, C. H. Cui, D. He, H. W. Liang, L. Wu, S. H. Yu, *Angew. Chem. Int. Ed*. 2013, **52**, 7472-7476.

6 a) S. Guo, S. Zhang, X. Sun, S. Sun, *J. Am. Chem. Soc.* 2011, **133**, 15354-15357; b) J. Luo, L. Y. Wang, D. Mott, P. N. Njoki, N. Kariuki, C. J. Zhong, T. He, *J. Mater. Chem*. 2006, **16**, 1665-1673; c) F. Ren, C. Wang, C. Zhai, F. Jiang, R. Yue, Y. Du, P. Yang, J. Xu, *J. Mater. Chem. A* 2013, **1**, 7255-7261.

7 a) Y. X. Zhang, H. C. Zeng, *J. Phys. Chem. C* 2007, **111**, 6970-6975; b) H. Li, Y. J. Li, L. L. Sun, X. L. Zhao, *Electrochimi. Acta* 2013, **108**, 74-78; c) S. J. Guo, S. J. Dong, E. K. Wang, *ACS Nano* 2010, **4**, 547-555.

8 a) H. A. Esfahani, M. Imura, Y. Yamauchi, *Angew. Chem. Int. Ed.* 2013, **52**, 13611-13615; b) L. Wang, Y. Yamauchi, *Chem. Eur. J.* 2011, **17**, 8810-8815; c) L. Wang, Y. Yamauchi, *J. Am. Chem. Soc.* 2013, **135**, 16762-16765; d) Y. J. Song, R. M. Garcia, R. M. Dorin, H. R. Wang, Y. Qiu, E. N. Coker, W. A. Steen, J. E. Miller, J. A. Shelnutt, *Nano Lett.* 2007, **7**, 3650−3655; e) X. W. Teng, X. Y. Wang, S. Maksimuk, H. Yang, *Small* 2006, **2**, 249-253.

9 C. Li, M. Imura, Y. Yamauchi, *Phys. Chem. Chem. Phys.* 2014, **16**, 8787-8790.

10 H. H. Li, C. H. Cui, S. Zhao, H.-B. Yao, M. R. Gao, F. J. Fan, S. H. Yu, *Adv. Energy Mater*. 2012, **2**, 1182-1187.

11 S. V. Bagul, S. D. Chavhan, R. Sharma, *J. Phys. Chem. Solids* 2007, **68**, 1623-1629.

12 a) C. Li, Y. Yamauchi, Chem. Eur. J. 2014, 20, 729-733; b) D. Xu, S. Bliznakov, Z. Liu, J. Fang, N. Dimitrov, *Angew. Chem. Int. Ed.* 2010, **49**, 1282-1285.

13 a) D. Sun, G. Zhang, X. Jiang, J. Huang, X. Jing, Y. Zheng, J. He, Q, Li, *J. Mater. Chem. A* 2014, **2**, 1767-1773; b) W. Li, X. Zhao, T. Cochell, A. Manthiram, *Appl. Catal. B: Environ.* 2013, **129**, 426-436; c) C. Wang, B. Peng, H. N. Xie, H. X. Zhang, F. F. Shi, W. B. Cai, *J. Phys. Chem. C* 2009, **113**, 13841–13846; d) Y. Jiang, Y. Jia, J. Zhang, L. Zhang, H, Huang, Z. Xie, L, Zheng, *Chem. Eur. J.* 2013, **19**, 3119–3124.

14 a) X. H. Zhong, Y. Y. Feng, W. Knoll, M. Y. Han, *J. Am. Chem. Soc*. 2003, **125**, 13559-13563; b) D. Xu, Z. Liu, H. Yang, Q. Liu, J. Zhang, J. Fang. S. Zou, K. Sun, *Angew. Chem. Int. Ed.* 2009, **48**, 4217–4221.

15 a) X. Yu, D. Wang, Q. Peng, Y. Li, *Chem. Eur. J*. 2013, **19**, 233-239; b) G. Wang, B. Huang, L. Xiao, Z. Ren, H. Chen, D. Wang, H. D. Abruña, J. Lu, L. Zhuang, *J. Am. Chem. Soc.* 2014, **136**, 9643-9649.

16 a) D. Wang, Y. Li, *J. Am. Chem. Soc.* 2010, **132**, 6280-6281; b) D. Wang, Y. Li, *Adv. Mater*. 2011, **23**, 1044-1060.

17 a) M. Gong, G. Fu, Y. Chen, Y. Tang, T. Lu, *ACS Appl. Mater. Inter*. 2014, **6**, 7301-7308; b) W. Chen, R. Yu, L. Li, A. Wang, Q. Peng, Y. Li, *Angew. Chem. Int. Ed.* 2010, **49**, 2917-2921; c) K. Lee, S. W. Kang, S. U. Lee, K. H. Park, Y. W. Lee, S. W. Han, *ACS Appl. Mater. Inter*. 2012, **4**, 4208-4214.

18 a) X. Wang, C. Liang, S. Dai, *Langmuir* 2008, **24**, 7500-7505; b) L. Wang, Y. Yamauchi, *J. Am. Chem. Soc*. 2009, **131**, 9152-9153; c) J. Wei, D. Zhou, Z. Sun, Y. Deng, Y. Xia, D. Zhao, *Adv. Funct. Mater*. 2013, **23**, 2322-2328; d) R. Liu, Y. Shi, Y. Wan, Y. Meng, F. Zhang, D. Gu, Z. Chen, B. Tu, D. Zhao, *J. Am. Chem. Soc.* 2006, **128**, 11652-11662.

19 a) S. Zhang, S. Guo, H. Zhu, D. Su, S. Sun, *J. Am. Chem. Soc*. 2012, **134**, 5060−5063; b) X. Huang, Y. Chen, E. Zhu, Y. Xu, X. Duan, Y. Huang, *J. Mater. Chem. A* 2013, **1**, 14449–14454; c) A. X. Yin, X. Q. Min, W. Zhu, W. C. Liu, Y. W. Zhang, C. H. Yan, *Chem. Eur. J.* 2012, **18**, 777-782; d) Y. Qi, T. Bian, S. I. Choi, Y. Jiang, C. Jin, M. Fu, H. Zhang, D. Yang, *Chem. Commun.* 2014, **50**, 560-562.

20 a) Y. Tong, H. S. Kim, P. K. Babu, P. Waszczuk, A. Wueckowski, E. Oldfield, *J. Am. Chem. Soc.* 2002, **124**, 468–473, b) C. Zhang, S. Y. Hwang, A. Trout, Z. Peng, *J. Am. Chem. Soc.* 2014, **136**, 7805−7808; c) S. I. Choi, S. Xie, M. Shao, J. H. Odell, N. Lu, H. C. Peng, L. Protsailo, S. Guerrero, J. Park. X. Xia, J. Wang, M. J. Kim, Y. Xia, *Nano Lett*. 2013, **13**, 3420−3425.

21 a) M. Wang, W. Zhang, J. Wang, A. Minett, V. Lo, H. Liu, J. Chen, J. *Mater. Chem. A* 2013, **1**, 2391–2394; b) L. X. Ding, A. L. Wang, G. R. Li, Z. Q. Liu, W. X. Zhao, C. Y. Su, Y. X. Tong, *J. Am. Chem. Soc.* 2012, **134**, 5730−5733; c) C. Li, B, Jiang, M. Imura, V. Malgras, Y. Yamauchi, *Chem. Commun*. 2014, **50**, 15337−15340.